SOLUTION MINING RESEARCH INSTITUTE
105 Apple Valley Circle
Clarks Summit, PA 18411, USA

Telephone: +1 570-585-8092
Fax: +1 505-585-8091
www.solutionmining.org

Technical Conference Paper

Stability Analysis of Natural-Gas Storage Caverns in Salt Formations

Amin Asgari, Ahmad Ramezanzadeh, Seyed Mohammad Esmaeil Jalali
Shahrood University of Technology, Shahrood, Iran

Benoît Brouard
Brouard Consulting, Paris, France

SMRI Fall 2012 Technical Conference
1-2 October 2012
Bremen, Germany

Solution Mining Research Institute Fall 2012 Technical Conference

Bremen, Germany, 1-2 October 2012

Stability Analysis of Natural-Gas Storage Caverns in Salt Formations

Amin Asgari, Ahmad Ramezanzadeh, Seyed Mohammad Esmaeil Jalali

Shahrood University of Technology, Shahrood, Iran

Benoît Brouard, Brouard Consulting, Paris, France

Abstract

Predicting rock salt behavior is crucial for an accurate and reliable design of underground storage caverns in salt formations, and specifically to ensure the stability and integrity of these underground spaces throughout project's entire operational life. This assessment should consider nonlinear and time-dependent behavior for rock salt under complicated loading conditions. Furthermore, as cyclic gas pressure and temperature changes must be integrated into the analyses, the application of suitable numerical methods is indispensable.

Different stability criteria are available to evaluate salt instability, including "No Tension", "No Tensile Effective Stress" and "No Dilation". These criteria, respectively, mean that no main stress and no effective tangential stress can be tensile. Also, no dilation can occur at cavern walls when considering a specific dilation criteria. To maintain cavern stability, all these criteria must be satisfied. In this study, numerical modeling has been performed utilizing LOCAS, a 2D axisymmetric finite-element code, to assess the effect of various operating and geometrical parameters on cavern behavior.

This paper will offer an overall assessment of the behavior of salt caverns used for natural gas storage. Specific loading scenarios will be considered first. Then, thorough parametric and sensitivity analyses will be used to investigate the impacts of the geometrical parameters (cavern depth, shape and volume) and operational parameters (max/min pressure, cycle's number, cycle's period and gas injection temperature) on the behavior of salt caverns.

This study shows that dilation occurrence is more likely to happen within the first cavern life cycle when pressure drops to the minimum level. As for the potential of tension occurrence in the surrounding rock, this is more likely to happen by increasing number of operation cycles, especially in the upper one-third of the cavern wall. Finally, it is seen that cavern depth and minimum cavern internal pressure are even more important influences on the salt cavern behavior.

Key words: Caverns for Gas Storage, Cavern Operation, Cavern Design, Computer Modeling

Introduction

During the last 50 years, storage in rock salt formations has developed rapidly. An increased number of gas storage caverns are in operation, characterized by increasing volume and increasing number of caverns per storage field. Knowledge and experience have been gained on how to design and operate storage volumes of up to 1 Mio m^3. Commonly, these are seasonal storages used as buffers for gas to supply periods of high demand (Minkley et al., 2011). As a result of the increasing use of such formations, additional knowledge and understanding of how to design safe storage caverns must be revised.

Salt domes have served as excellent hosts for the storage of oil and gas in underground caverns. The state of stresses around the cavern in these salt domes depends on the depth of the cavern (Initial stresses and rock mass temperatures increase with depth.), the primary stress state of the rock mass, the

internal gas pressure in the cavern, and the injection and withdrawal rates during these cycles (thermodynamic processes). Furthermore, salt creep behavior and cavern geometry influence stress redistributions during loading and unloading phases.

The thermodynamic processes involved in a gas-storage cavern include the heating and cooling caused by gas compression and expansion, heat transfer between the gas and the surrounding rock, and energy changes caused by mass flow into and out of the cavern that finally leads to temperature changes of the gas in the cavern. Because salt has a relatively high thermal-expansion coefficient (Staudtmeister and Zapf, 2010), large changes in gas temperature leads to the creation of significant thermal stresses at the cavern wall (Lestringant et al., 2010). For this reason, the stability criteria must be revisited, especially in terms of tension as well as shear load condition.

The following stability criteria were provided by Brouard et al. (2007): (1) no, or small, dilatant zone; (2) no, or small, tensile zone; (3) no, or limited, effective tensile zone; (4); limited volume loss and volume loss rate; and (5) limited subsidence (Lestringant et al., 2010, Brouard et al., 2011).

The objective of this paper is to present an overall assessment of the behavior of salt caverns that are used to store natural gas (on the baseline model) and, then, by using thorough parametric and sensitivity analyses of gas caverns with respect to cavern geometry (cavern depth, shape and volume) and operation pattern (max/min pressure, cycle number, cycle period and gas injection temperature), to investigate the impacts of these parameters on salt cavern behavior.

Rock mass structure, cavern geometry, material behavior and cavern operation patterns require complex physical models to describe the load-bearing behavior of the geomechanical structure. The determination of stress, strain and deformation in the rock mass due to cavern construction and operation is only possible with help of numerical tools such as the Finite Element Method (FEM) or Finite Difference Method (FDM). Consideration of thermal effects are not conventional in the numerical simulations for seasonal storage modes (Zander-Schiebenhöfer, 2010). In this study, thermo-mechanical coupled calculations are performed. Generally, it is sufficient to use axisymmetric models for the numerical calculations of caverns in rock salt, especially in the design of new caverns.(Riekenberg et al., 2010)

For this paper, the FEM computer 2D axisymmetric code LOCAS is used for numerical simulations. LOCAS is able to calculate the thermo-elastic stresses that are triggered by cycles in the vicinity of cavern wall and to perform coupled thermal, hydraulical and mechanical computations at the same time.

Baseline Model

Geological Structure

A typical salt-dome stratigraphy was used for the simulations. The geologic formation is assumed to be entirely salt within a range of depth between 200 m and 2200 m (table 1). A schematic of the baseline cavern design is shown in Figure 1. Initial state of stress is assumed to be isotropic and equal to the weight of the overburden. A ground surface temperature of 25°C and a geothermal gradient of 0.0187°C per meter of depth were assumed. (DeVries et al., 2002).

Table 1. Stratigraphy and geomechanic properties of layers used for the simulations.

Layer No.	Type	Thickness (m)	Density (kg/m^3)	Young's Modulus (GPa)	Poisson's Ratio
1	Overburden	200	2600	40	0.35
2	Salt	2000	2200	30	0.25

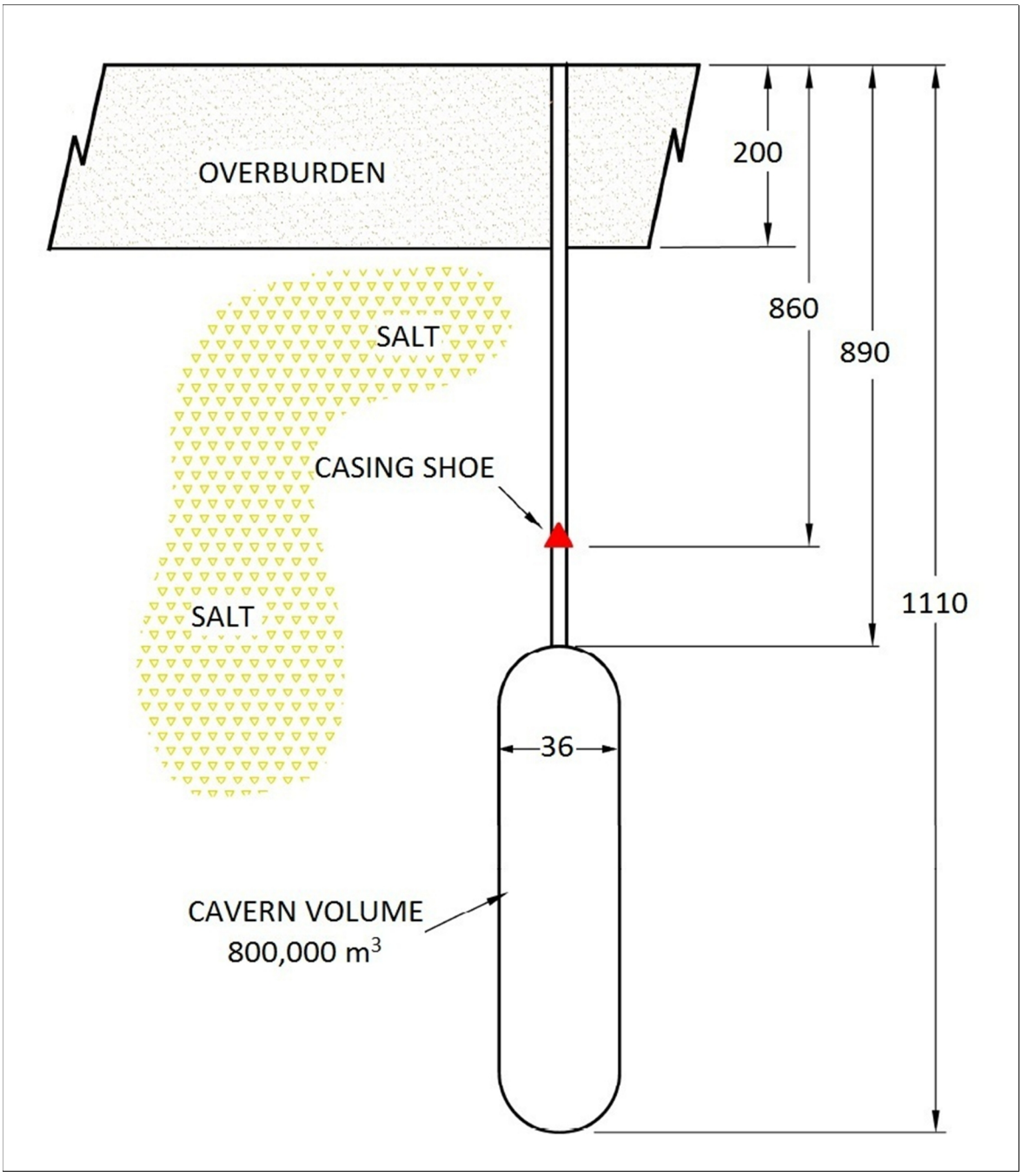

Figure 1. Schematic of Baseline Cavern Model. (after Nieland, 2008).

Geomechanical characteristics and constitutive law

The constitutive law for salt should incorporate transient creep and be temperature-dependent. Munson and Dawson (1984) suggested the now well-known model:

$$\dot{\varepsilon}^{ij} = \dot{\varepsilon}_e^{ij} + F\dot{\varepsilon}_s^{ij} \qquad \begin{cases} F = e^{\Delta\left(1-\varsigma/\varepsilon_t^*\right)^2} & \text{when } \varsigma \le \varepsilon_t^* \\ F = e^{-\delta\left(1-\varsigma/\varepsilon_t^*\right)^2} & \text{when } \varsigma \ge \varepsilon_t^* \end{cases} \tag{1}$$

$$\begin{cases} \dot{\varsigma} = (F-1)\dot{\varepsilon}_{ss} \quad \dot{\varepsilon}_{ss} = A\exp\left(-\frac{Q}{RT}\right)(\sqrt{3J_2})^n \qquad \mu = E_{salt}/2(1+\nu_{salt}) \\ \varepsilon_t^* = K_0 e^{cT}\sigma^m \quad \Delta = \alpha_w + \beta_w\, Log_{10}\left(\frac{\sigma}{\mu}\right) \quad \sigma = \sqrt{3J_2} \end{cases} \tag{2}$$

Table 2 shows parameters for Avery Island salt. Table 2 and table 3 respectively give typical thermal properties of salt and natural gas assumed for the simulations (Brouard et al., 2011 and 2007b)

Table 2. Considered mechanical and thermal parameters.

Munson- Dawson Model Parameters				Thermodynamic Parameters		
	Parameter	**Unit**	**Value**	**Parameter**	**Unit**	**Value**
Steady State Creep	A	$MPa^{-n}.yr^{-1}$	0.74	Thermal Capacity	$J.kg^{-1}.K^{-1}$	921
	n	-	5	Thermal Diffusivity	$\times 1E10^{-6}\ m^2.s^{-1}$	3
	Q:R	K	5032			
Transient Creep	m	-	3	Thermal Conductivity	$W.m^{-1}.^{\circ}C^{-1}$	6.08
	[illegible]	-	-13.2			
	[illegible]	-	-7.738	Thermal Expansion Coefficient	$\times 1E10^{-4}\ ^{\circ}C^{-1}$	4
	K_0	MPa^m	7×10^{-7}			
	[illegible]	-	0.58			
	c	K^{-1}	9.02×10^{-3}			

Table 3. Thermodynamics properties of natural gas.

Parameters	Unit	Value
Temperature reference	K	293.15
Pressure reference	atm	1
Density	$Kg.m^{-3}$	0.67
Thermal Capacity C_p	$J.kg^{-1}.K^{-1}$	2168.6
Thermal Capacity C_v	$J.kg^{-1}.K^{-1}$	1683
Ratio C_p/C_v	-	1.296
Dynamic Viscosity	$\times 1E10^{-5}$ Pa.s	1.025

Cavern geometry and Meshing

The results presented in this paper are based on the simulation of a 800,000 m3 (5 MMbbls) cavern. The cavern is capsule-like in shape, 220 m tall, and has a maximum radius of 36 m. Table 4 gives the cavern geometry and meshing parameters. The mesh used for numerical computation is shown on Figure 2.

Table 4. Cavern geometry and meshing parameters.

Baseline Geometry Parameters		Meshing Parameters	
Cavern Shape	Capsule	Elements	13777
H:D ratio	3	Nodes	7220
Cavern Volume (m^3)	8×10^5	Height (m)	2200
Cavern Max. Radius (m)	36	Width (m)	1000
Average Cavern Depth (m)	1000	Av. Distance Between Nodes on Wall (m)	0.5
Top Cavern Depth (m)	890		
Casing Shoe Depth (m)	860		

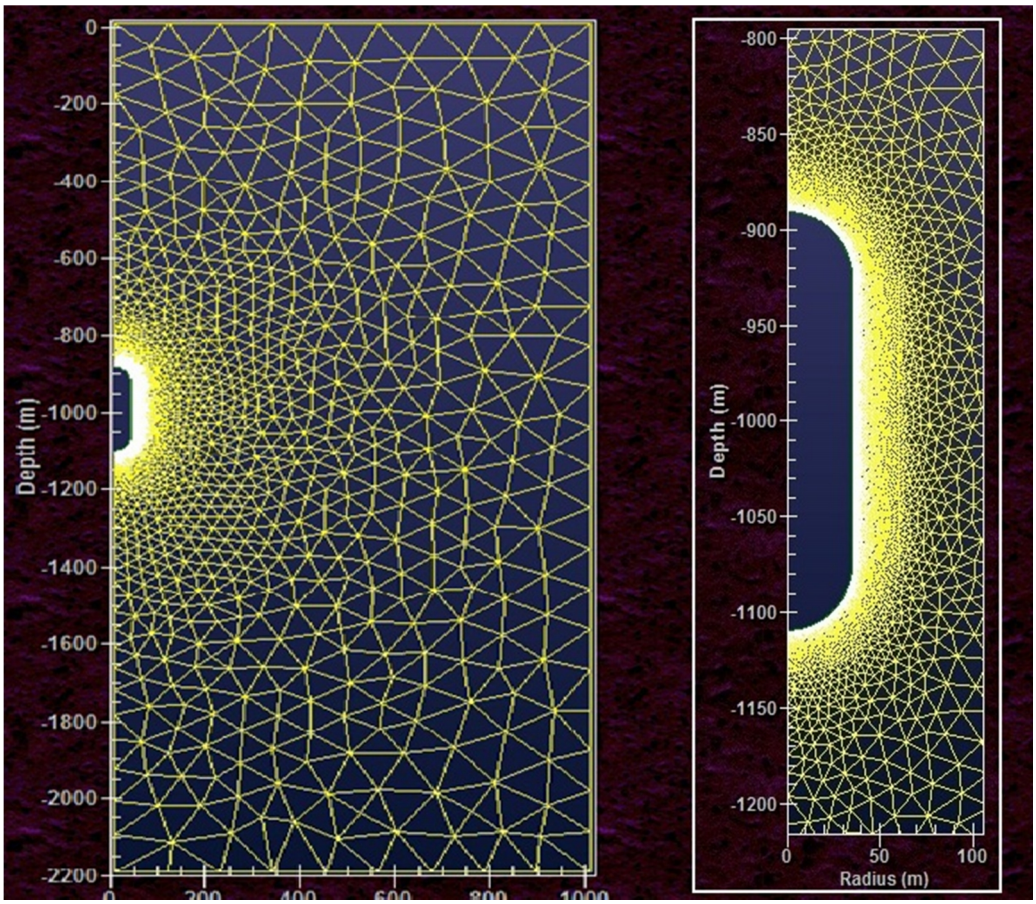

Figure 2. Mesh used for numerical analysis.

Cavern History

The baseline annual gas-storage cycle (cavern pressure history) is represented on Figure 3. In all of the simulations performed, the casing seat was assumed to be 30 m above the top of the cavern. All of the gas-storage simulations were preceded by a cavern leaching phase (2 years) and a dewatering phase (1 year). During the creation period, cavern pressure decreases from geostatic (22.4 MPa) to halmostatic (11.5 MPa, point No.1 in Figure 2); during dewatering, cavern pressure reached 16.5 MPa (i.e., a pressure gradient of 0.85 psi/ft at the casing-shoe depth, point No. 2 in Figure 2), after which the cavern can be operated as storage for natural gas.

Each of the turns in the cycle include withdrawal of the working gas over a period of 150 days, followed by injection of the working gas over a 215-day period. For the baseline cavern, with a minimum casing-seat pressure gradient of 0.20 psi/ft (4.5×10^{-2} MPa/m), the pressure at the cavern top is 4.5 MPa (points No. 3 and 4 in Figure 3). At the maximum baseline casing-seat pressure gradient of 0.85 psi/ft, the pressure at the cavern top is 16.5 MPa (point No. 5 in Figure 2). To achieve a nearly steady-state thermal cycle in the cavern, the annual gas cycle was repeated continuously for 10 years. Also, the injection temperature of the gas was assumed to be 37 °C.

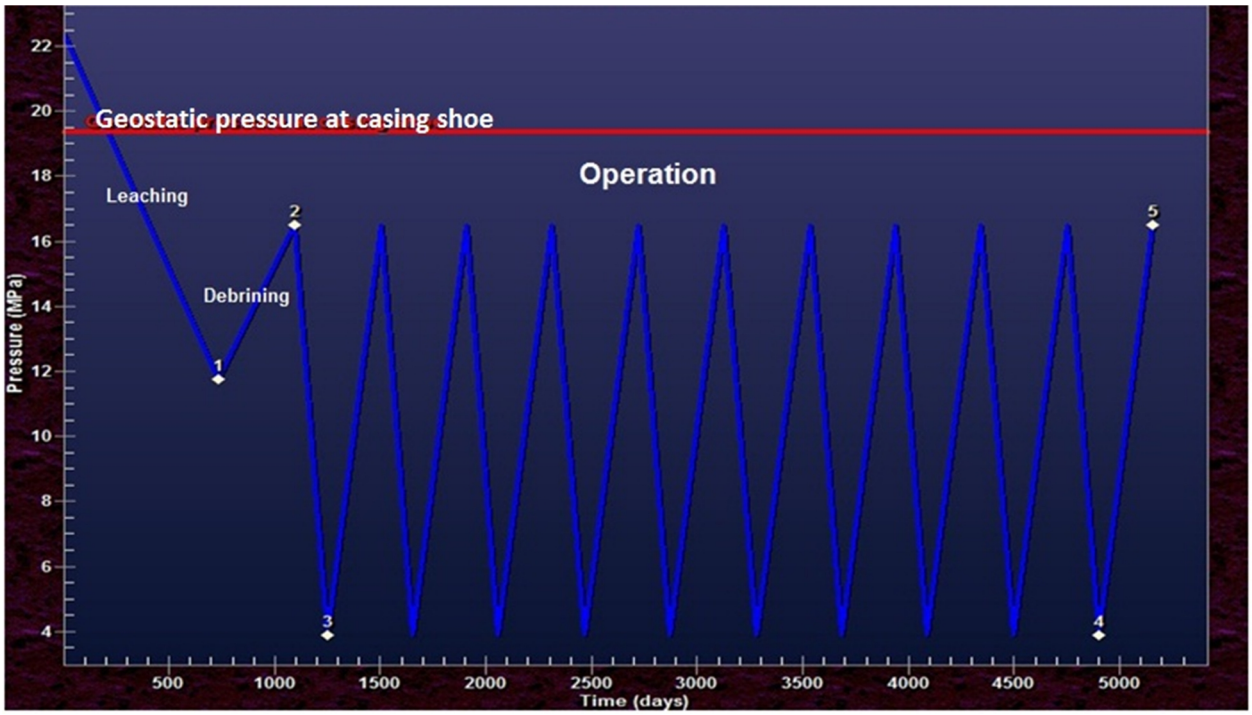

Figure 3. Considered cavern pressure history.

Stability Criteria

When working with cycling loading and cavern stability, the onset of tensile stresses and salt dilation at the cavern wall must be considered. The tensile strength of salt is low, and large tensile stresses lead to roof or wall spalling. For this reason, tensile zones must be avoided (i.e $\sigma_{\theta\theta} < 0$). In addition, the effective tangential stress at the cavern wall must be negative (i.e $\sigma_{\theta\theta} + P < 0$ where P is cavern gas pressure).

Cavern volume loss and subsidence are closely related. Cavern volume loss rate must be typically limited to 1% per year.

Cavern volume loss and subsidence are closely related. The cavern volume-loss rate typically is limited to 1% per year.

When shear stresses are large (compared to the mean stress), salt micro-fracturing and dilation take place, which leads to an increase in permeability and a loss of rock strength (Brouard et al., 2011). For this reason, a large dilatant zone must be avoided.

The considered dilation criterion is the DeVries (DV) criterion (DeVries et al., 2005), which is defined as:

$$\sqrt{J_2} < \sqrt{\mathrm{J}_{2\,\mathrm{dil}}} = \frac{D_1 \left(\frac{|I_1|}{sgn(I_1)\sigma_0}\right)^m + \bar{T}_0}{\sqrt{3}\cos\theta - D_2 \sin\theta}$$

Where $\sigma_0 = 1$ MPa is a dimensional constant, $\bar{T}_0$ is the unconfined tensile strength of salt, ψ is lode angle, and (D_1 ،D_2 ،m) are salt parameters. Dilation appears when Factor of Safety (FOS) falls below 1:

$$FOS = \frac{\sqrt{\mathrm{J}_{2\,\mathrm{dil}}}}{\sqrt{\mathrm{J}_2}} < 1$$

Table 5 gives the DV dilation criteria parameters selected for this study (DeVries et al., 2002).

Table 5. DeVries dilation criterion parameters for Cayuta salt.

Parameters	Unit	Value
T_0	MPa	1.95
m	-	0.693
D_1	-	0.773
D_2	-	0.524

Stability Analysis of the Cavern Baseline Model

The salt surrounding the cavern is analogous to a constant temperature heat source or heat sink, depending on whether the cavern gas temperature is above or below the salt temperature.

With increasing numbers of storage cycles, when the gas temperature is higher or lower than the in-situ salt temperature, heat will be transferred between the cavern and the surrounding salt so that the average cavern temperature changes to obtain balance with the geothermal temperature. From Figure 4, it can be concluded that the effect of decreasing pressure (withdrawal phase) on cavern temperature is greater than increasing pressure (injection phase) results in more thermal stress being induced in the withdrawal phase. A 12.5-MPa pressure change between max/min cavern pressures results in a 21 °C temperature changes at the cavern wall.

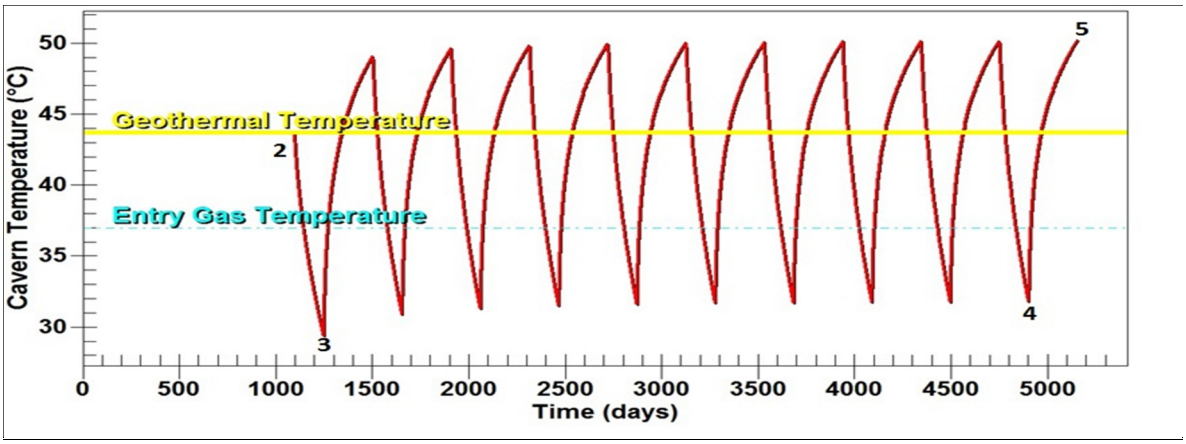

Figure 4. Computed evolution of cavern temperature.

Along the cavern wall

Figure 5 shows stress distribution in terms of least principal stress along the cavern wall for selected times in the cavern history (see Figure 3). The area most vulnerable to tensile failure is the cylindrical part of the cavern, where, cavern at the time at which the cavern pressure is at lowest value. The maximum principal stress at this part of cavern reaches –0.5 MPa at the10th minimum pressure. Nevertheless, stresses remain compressive at the cavern wall during the cavern's life. It can be observed that, at the end of leaching and debrining, and during the first minimum pressure, the distribution of least-compressive stress at the cavern wall is uniform. After the 1st minimum pressure, the tensile stress distribution on the cavern wall is almost non uniform and increases with increasing cycles.

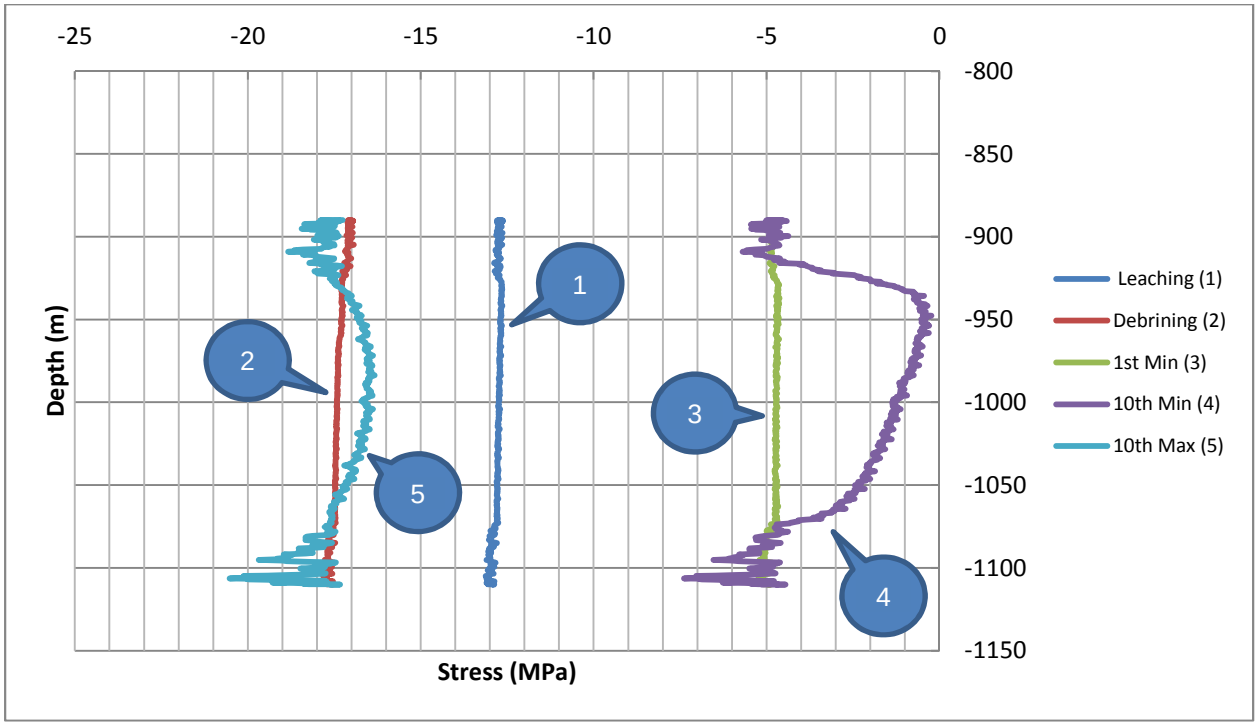

Figure 5. Least principal-stress distribution along the cavern wall.

Figure 6 shows stress distribution in terms of effective stress along the cavern wall for selected times in the cavern's history (see Figure 3). The area most vulnerable to effective tensile failure is at the bottom of the cavern roof, at a depth of 950 m. where, cavern at the time at which the cavern pressure is at lowest value. It can be observed that, at the end of leaching and debrining, and during the first minimum pressure, the distribution of effective stress at the cavern wall is uniform and in a compressive state. As shown in Figure 6, the area most vulnerable to tensile failure is the cylindrical part of the cavern, where, cavern at the time at which the cavern pressure is at lowest value the cavern pressure is at its lowest value. At the 10th minimum pressure, the middle part of the cavern wall is in tensile mode, which means the developing tensile area at the cavern wall is most likely when the number of storage cycles increases. It should be noted that during the cavern life, the state of effective stress remains compressive in the upper and lower spherical parts of the cavern wall.

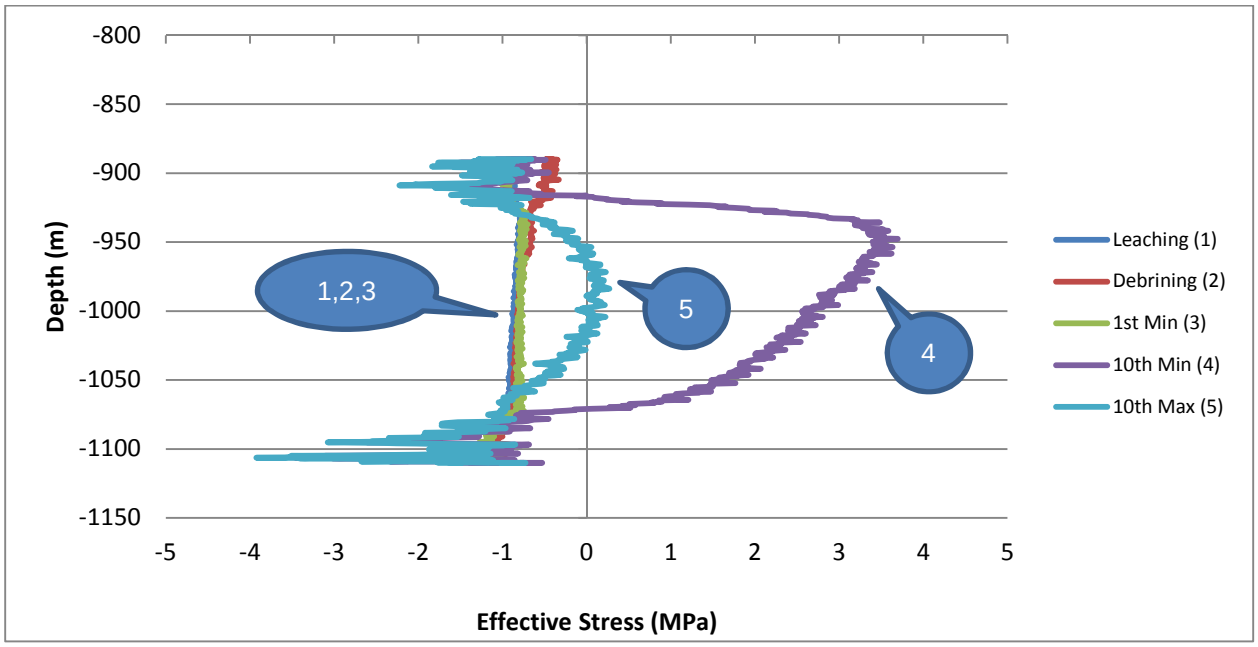

Figure 6. Effective stress distribution along the cavern wall.

Figure 7 shows evolution of stress state as a function of shear stresses and mean stresses (invariants plane). The state of stress is computed at the cavern wall, at a 1000–m depth (Point D in Figure 7). The state of stress is "normal" except during short period of times when the considered point at the cavern wall experiences dilatancy. Another computation is performed for other parts of cavern wall, roof, bottom and casing-shoe area (Points A, B, C, E and F in Figure 7). When comparing these points, it observed that dilatancy is more likely to happen at middle height of cavern wall (1000-m depth).

Along the radial direction

Figure 8 shows radial stress distribution in terms of least-compressive principal stress along the radial direction at middle height of the cavern (i.e., at a 1000-m depth) for selected times in cavern history (see Figure 3).

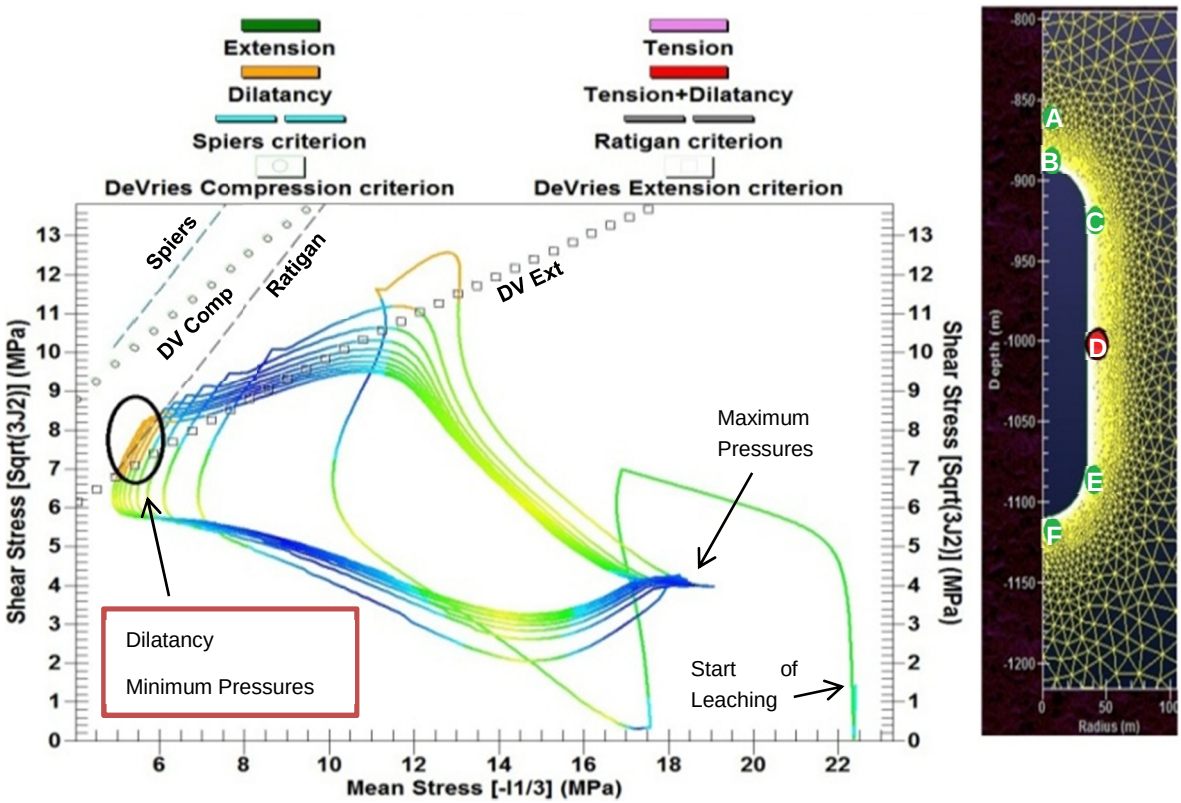

Figure 7. Evolution of stress state at the cavern wall 1000-m depth (Point D).

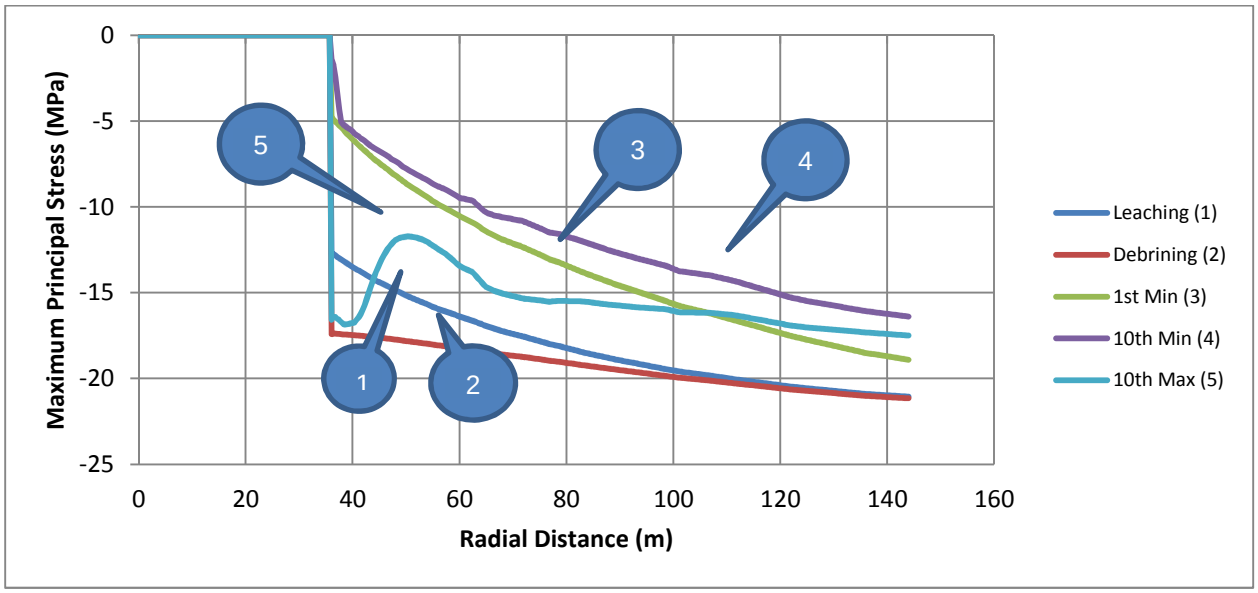

Figure 8. Radial distribution of the least-compressive principal stress at a 1000-m depth.

Figure 9 shows radial stress distribution in terms of effective stress along the radial direction at mid-height (1000 m) for selected times in cavern history (see Figure 3).

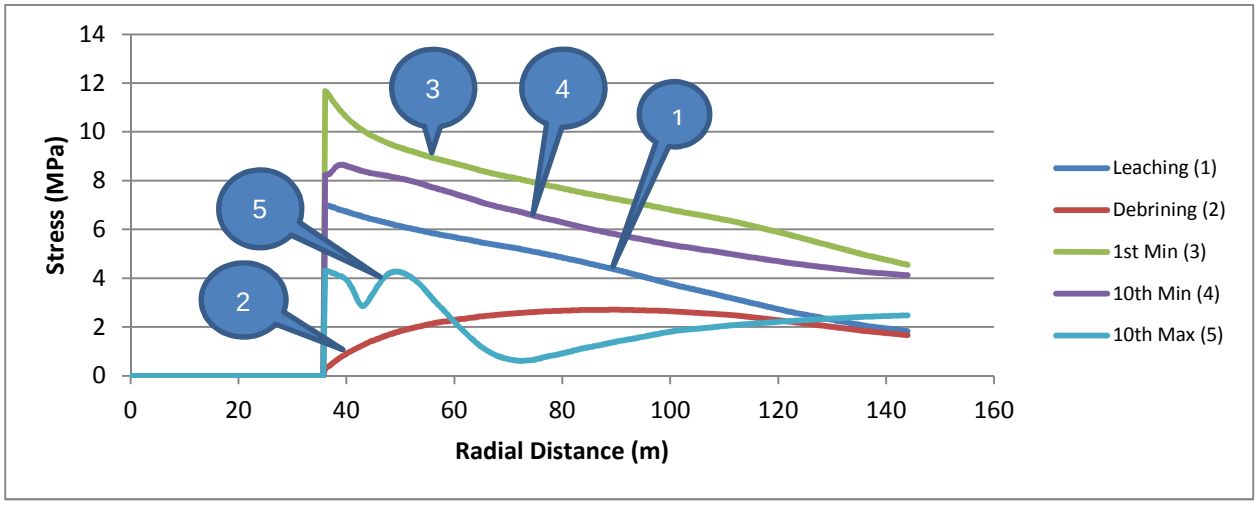

Figure 9. Effective stress distribution along the radial direction at 1000 m.

Figure 10 shows salt dilation potential considering the DV criteria along the radial direction at cavern mid-height FOS is plotted for selected times in the cavern history.

During cavern life, no dilation occurs, and the minimum FOS is larger than 1. In the distance of two times cavern radius from cavern wall, the FOS for the first and 10th minimum pressures is less than 2. Also, along the radial direction in the surrounding salt, the FOS for the 10th minimum pressure is greater than first minimum pressure (i.e., $FOS_{10th} > FOS_{1st}$).

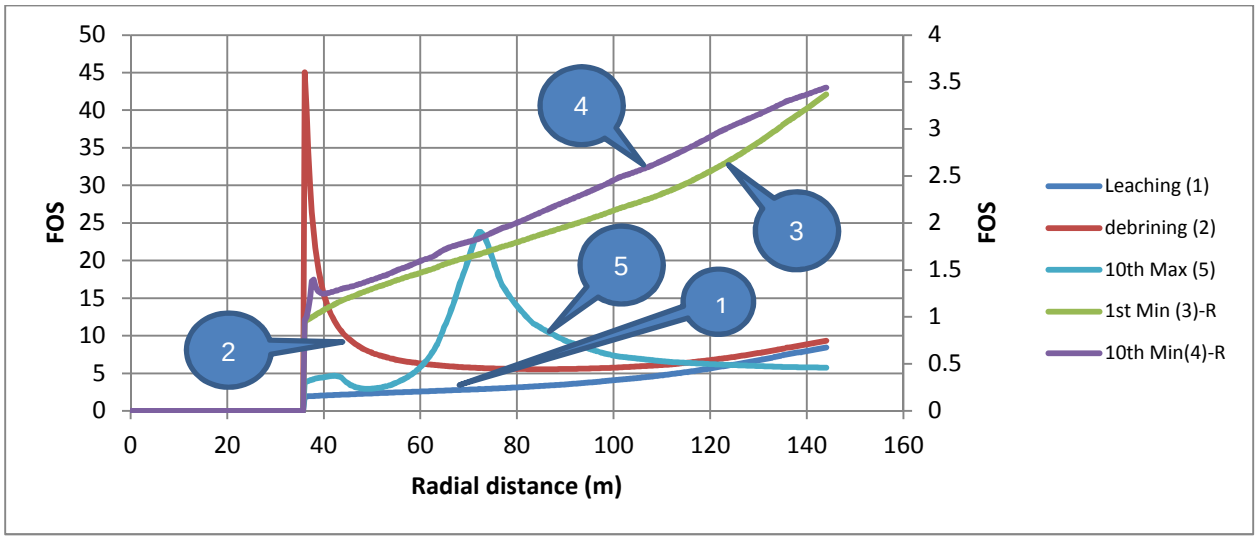

Figure 10. Dilation states along the radial direction at 1000-m depth as Factor of Safety (FOS); for R, refer to right-side vertical axis.

Along the vertical direction

Figure 11 shows vertical stress distribution along the cavern axis above the cavern in terms of least-compressive principal stress for selected times in the cavern history.

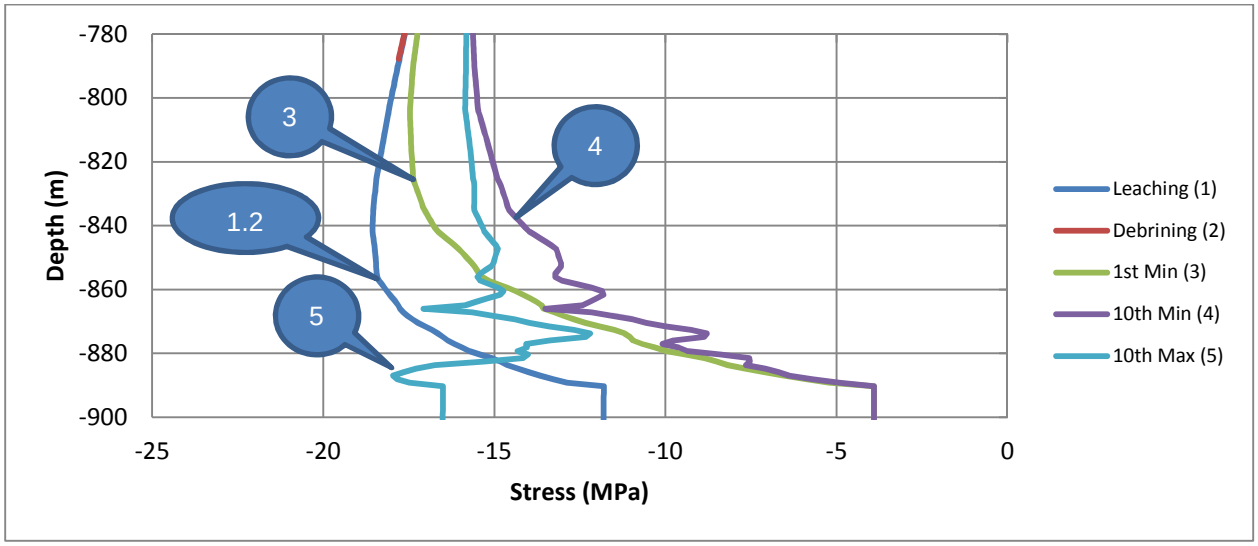

Figure 11. Least-compressive principal stress distribution along cavern axis direction.

Figure 12 shows the potential of dilation (DV criteria) of salt rock along cavern vertical axis as factor of safety (FOS). When the pressure is minimum in the cavern, the confining stress is low, and the deviatoric stress is high; therefore, the risk of dilation is maximum (FOS near 1). Conversely, there is no risk of dilation in the salt mass when the cavern pressure is maximum.

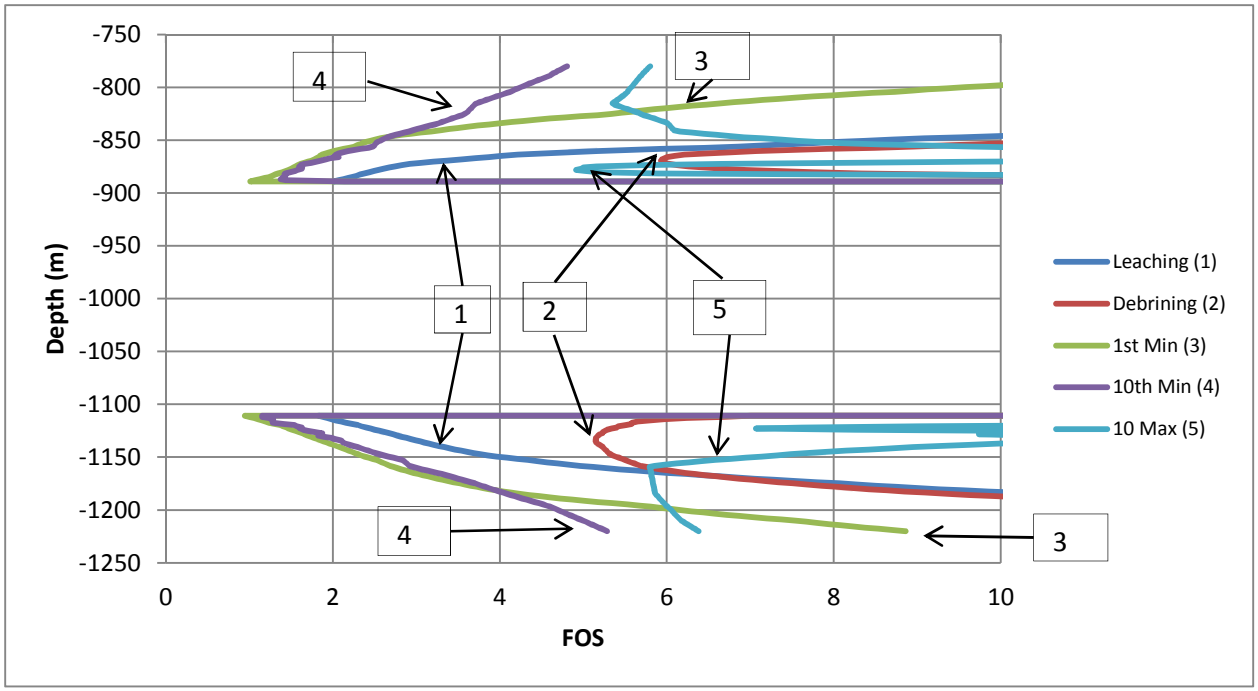

Figure 12. Potential distribution of dilation along the vertical axis as Factor of Safety (FOS).

At the casing-shoe area

Figures 13, 14 and 15 show evolution of least-compressive principal stress, effective stress and dilation potential (DV criteria), respectively, at the casing-shoe area. The variations of the least-compressive stress, effective stress and dilation potential in the casing-shoe area are shown in Figures 12, 13, and 14, respectively. As shown in Figure 12, the least-compressive stress variations increase as the number of cycles increases. The least-compressive stress in the cavern is highest at the 10th minimum pressure. As shown in Figure 13, tensile effective stresses are likely to develop at the casing-shoe area, where, cavern at the time at which the cavern pressure experiences a large pressure increase. Also, effective stress variations increases as the number of cycles increases, (It is highest at the 10th maximum pressure cycle).

The next parameter evaluated was dilation potential. Figure 14 shows the evolution of dilation potential (DV criteria) at casing-shoe area. Dilation-potential variations decreases as the number of turns increases. Thus, it can be said that dilation-potential is likely to develop at the casing-shoe area during the first cavern life cycles, where, cavern at the time at which the cavern pressure drops to the minimum level.

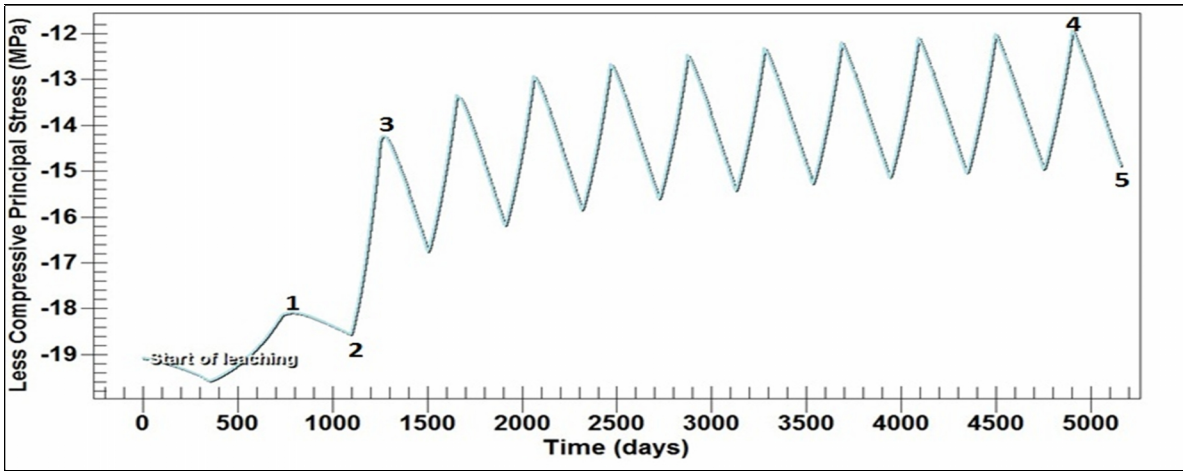

Figure 13. Evolution of least-compressive principal stress at the casing-shoe area.

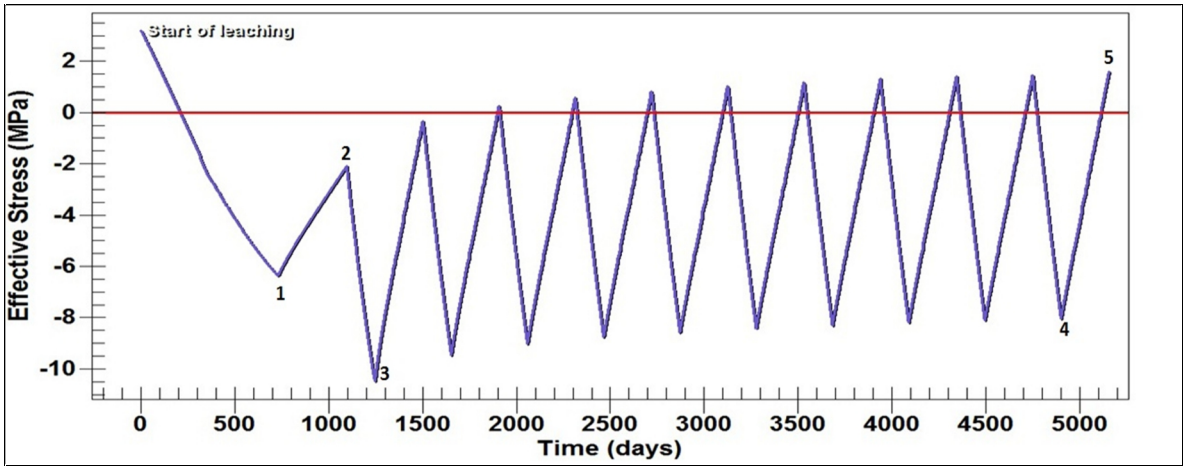

Figure 14. Evolution of effective stress at the casing-shoe area.

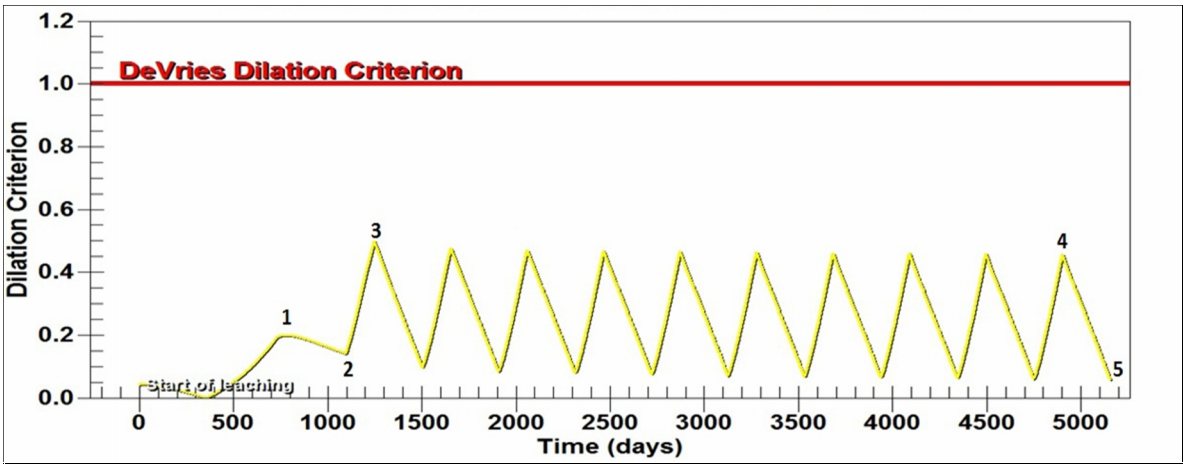

Figure 15. Evolution dilation potential (DV criteria) at the casing-shoe area.

Sensitivity Analysis

Table 6 present the baseline set of typical operational and design parameters chosen for the sensitivity analysis. The effects of the parameters on the stability of salt rock around the casing-shoe area were examined for cavern depth, cavern shape, cavern volume, minimum pressure gradient, maximum pressure gradient, cycle number, cycle period and gas injection temperature.

Each of the baseline parameters was varied to determine the effect of the parameter on the stability criteria for salt rock around the casing-shoe area. It should be noted that, from geomechanical or regulatory perspectives, the range of cavern design parameters used in these analyses may or may not be possible.

Table 6. Parameters considered for the sensitivity analysis.

Type	Check Effect	Unit	Range					
					Baseline			
Geometry	Cavern Depth	m		500	1000	1500		
	Cavern Shape	H:D ratio		1	3	5	7	9
	Cavern Volume	1E5 m^3		4	8			
Operational	Min Pressure	psi/ft			0.2	0.3	0.4	
	Max Pressure	psi/ft	0.75	0.80	0.85			
	Cycle's Number	-			10	20		
	Cycle's Period	Day	30	180	365			
	Gas Injection Temperature	$^{\circ}C$		21	37	54		

Table 7 lists the correlation between the parameters and their impact on the stability of salt rock in the casing-shoe area with respect to stability criteria (includes No Tension, No Effective Tension, Dilation and Cavern Loss Volume Rate). An upward pointing arrow (↑) indicates an advantageous impact; a downward pointing arrow (↓) indicates a disadvantageous impact.

We can obtain useful clues from Table 7 for geometrical and operational parameters by anticipating the degree to which the parameters impact the stability of salt rock in the casing-shoe area and cavern volume-loss rate.

Considering cavern volume-loss rate, the cavern depth and minimum pressure, among other parameters, have the largest impact on the rate of cavern volume-loss. As expected, increasing cavern depth will result in an increase of cavern volume-loss rate. The reverse is true when the minimum pressure increases.

The first baseline parameter evaluated is cavern depth. In these simulations, the average depth of the cavern was varied from 500 m to 1,500 m, which has a very significant impact on cavern stability. Increasing the cavern depth increases the tensile stresses at the casing-shoe, but it also reduces the potential of developing effective tensile stresses and dilation.

As shown in the Table 7, the minimum gas pressure has a large impact on cavern stability at the casing-shoe area. Lowering the minimum gas pressure not only increases the development of tensile stresses, but also increases dilation potential in the vicinity of the casing-shoe.

Table 7. Correlation table- (↑): Advantage, (↓): Disadvantage.

Type	Check Effect	Stability Criteria			
		Volume Loss Rate (% per year)	at the Casing-shoe Area		
			S_{least}	S_{eff}	Dilation (DV)
Geometry	Cavern Depth (↑)	↓	↑	↓	↓
	Cavern Shape (↑)	↓	↑	↑	↑
	Cavern Volume (↑)	↓	↓	↓	↓
Operational	Min Pressure (↑)	↑	↑	↑	↑
	Max Pressure (↑)	↑	-	↓	-
	Cycle's Number (↑)	-	↓	↓	-
	Cycle's Period (↑)	↑	↓	↓	↑
	Gas Injection Temperature (↑)	↓	↓	↑	-

In contrast to the minimum gas-pressure effect, the maximum gas-pressure changes have limited impact on the stability of salt rock at casing-shoe area.

The next parameter evaluated is cavern shape which was introduced with a height-to-diameter (H:D) ratio. Increasing the H:D ratio has a positive impact on stability of salt rock at casing-shoe area. In other words, taller cavern are more stable than others. It should be noted that, in this study, the pressure

gradients were assumed to remain at the baseline values of depth at the casing-seat. Thus, increasing the H:D ratio will result in decreasing the value of pressure in the cavern.

Increasing the number of pressure cycles from 10 to 20 results in developing tensile stress and tensile effective stress at the casing-shoe area.

Increasing the cycling period from 30 days (12 cycles per year) to 365 days (1 cycle per year) results in increasing development of tensile and effective tensile stresses and in reducing dilation potential at the casing-shoe area.

The last parameter considered is the gas-injection temperature. Variations of this temperature have a very limited impact on the stability of salt in the casing-shoe area.

Conclusions

This study shows that dilation is more likely to occur during the first cycle of cavern life when pressure drops to the minimum. The potential of tension in surrounding rocks is more likely to occur when the number of cycles increases, especially at the upper one-third of the cavern wall. When considering a long period of time, due to the viscose characteristics of salt, a decrease in the deviatoric stress can be observed.

A sensitivity study was performed utilizing a 2D axisymmetric finite-element software to assess the effect of various cavern geometry and operational parameters in salt domes. The goal was to examine impacts of these parameters on the stability of rock salt in the casing-shoe area and on the cavern volume-loss rate.

Variations in the cavern design parameters (minimum pressure and cavern depth) have the largest impact on the stability of rock salt at the casing-shoe area.

Acknowledgements

Authors wish to acknowledge the supportive of this study by National Iranians Gas Company (NIGC).

References

Brouard B. Bérest P. and Karimi-Jafari M., 2007. Onset of tensile effective stresses in gas storage caverns, Fall 2007 Conference, 7-10 October, Halifax, Canada.

Brouard B., Karimi-Jafari M., Bérest P. and Durup G., 2007-b. Pressure Build-up in a Sealed Cavern: he Effect of a Gas Blanket. SMRI Spring 2007 Conference. Basel, Switzerland.

Brouard B. Frangi A. and Bérest P., 2011. Mechanical Stability of a Cavern Submitted to High-Frequency Cycles, SMRI Spring 2011 Technical Conference, Galveston, Texas, USA.

DeVries K.L., Mellegard K.D. and Callahan G.D., 2002. salt Damage Criterion Proof-of-Concept research.

DeVries K.L. Mellegard K.D. Callahan G.D. Goodman W.M., 2005. Cavern roof stability for natural gas storage in bedded salt. Final Report. Contract DE-FG26-02NT41651. Prepared for United States Department of Energy.

Lestringant C. Bérest P. and Brouard B., 2010. Thermo-mechanical effects in compressed air storage (CAES), SMRI Fall 2010 Technical Conference, Leipzig, Germany.

Minkley W. Lindert A. and Brückner D., 2011. The improved IfG Gas Storage Cavern Design Concept, SMRI Fall 2011 Technical Conference, 3–4 October 2011, York, United Kingdom.

Nieland J.D., 2008. Salt Cavern Thermodynamics-Comparison Between Hydrogen, Natural Gas, and Air Storage, SMRI Fall 2008 Technical Conference, 13–14 October 2008, Galveston, Texas, USA.

Riekenberg, R. Hartmann, U. Staudtmeister, K. Zander-Schiebenhöfer, D., 2004. Recommendation of maximum cavern pressures for the gas storage caverns at Huntorf on the basis of three- dimensional numerical models, Fall 2004 Technical Conference, 3 – 6 October, Berlin, Germany.

Staudtmeister K. and Zapf D., 2010. Rock Mechanical Design of Gas Storage Caverns for Seasonal Storage and Cyclic Operations, SMRI Spring 2010 Technical Conference, Grand Junction, Colorado, USA.

Zander-Schiebenhöfer D., 2010. High Frequency Cycling of Gas Storage Caverns Phase I Development of Appropriate Lab Tests & Design Criteria, SMRI Research Report RR2010-01.